Biol. Cybern. 87, 428–439 (2002)
DOI 10.1007/s00422-002-0354-x

Biological Cybernetics

Mapping time

C. Leibold, J.L. van Hemmen

Physics Department, TU München, 85747 Garching bei München, Germany

Received: 28 June 2002 / Accepted: 9 July 2002

Abstract. Neuronal coding of temporal stimulus features can occur by means of delay lines. Given that neuronal activity is conducted through many parallel axons, there has to be a mechanism guaranteeing minimal temporal dispersion. We argue that plastic changes in synaptic transmission that are unspecifically propagated along presynaptic axons are a basis for the development of delay-line topologies. Furthermore, we show how two populations of afferents form a map of interaural time differences as found, for instance, in the laminar nucleus of the barn owl.

1 Introduction

How is time represented by neuronal activity? This challenging question has fascinated neuroscientists already decades ago. A traditional way of thinking is to translate time into the place of high firing rate (Jeffress 1948) – a rate-place code of temporal features which we refer to as a temporal map. What is needed for any neuronal representation of time is a mechanism that translates time into a biophysical concept provided by the neuronal system, such us conduction delays, oscillation periods, decay times, or trajectories of network dynamics. In this paper we discuss the strategy of mapping time into a place code by means of delay lines.

Let us imagine a piece of neuronal tissue forming a functional unit with a spatial extent X, typically in the range of one to two millimeters. Afferent fibers pass through this set of cells in a prominent direction and are assumed to contact the cells synaptically (see Fig. 1).

The feedforward activity is propagated at a conduction speed c of at least 2 m/s. The time delay Λ across the area is thus of the order of $\Lambda = X/c \lesssim 5$ ms. A temporal map – i.e, a continuous representation of a stimulus feature along the arborization direction of the delay lines – is therefore restricted to a time scale of a few milliseconds. The neurons' average distance, denoted by δx, defines the temporal resolution of the spatial code through $\delta x/c$.

The neuronal delay of axon n at the edge of the nucleus is labeled Δ_{n0}. In order to guarantee the temporally most-precise propagation of postsynaptic excitation across the nucleus, the distribution width of edge delays Δ_{n0} has to be at least as small as the postsynaptic membrane time constants. The latter then determine the temporal resolution of the system.

Especially auditory brainstem neurons are very fast. Their postsynaptic potentials have rise times in the range of 100 μs. It is thus essential for the delay-line hypothesis to provide a mechanism that "tunes" delay distributions in an appropriate fashion. In this paper we concentrate on delay selection, meaning that an initially (in the immature animal) broad range of available delays Δ_{n0} is refined by "selecting" afferents with approximately the same delay and withdrawing the rest. Selection and withdrawal are both performed at the synaptic level. A synapse is said to be selected if its efficacy J has reached a stable high value, whereas it is withdrawn if J has vanished. The temporal dynamics of synaptic weights is governed by a learning rule (Gerstner et al. 1996; van Hemmen 2000), which originally dates back to Hebb (1949). The above paradigm is thus often referred to as Hebbian delay selection (Gerstner et al. 1996; Eurich et al. 1999; Leibold et al. 2002; Sect. 2). Since it explains the temporal evolution of synaptic efficacies at the level of a single neuron, the concept of delay selection has to be generalized to a whole afferent fiber. Here we will explain how this can be realized through so-called axon-mediated synaptic learning (AMSL; Sect. 3).

Theoretical discussion of synaptic dynamics will be performed by means of a Poisson neuron (Kempter et al. 1999; van Hemmen 2000), a neuron model that enables us to find explicit expressions for rate and correlation functions (Leibold et al. 2002; Sect. 4). We will show that, under the assumption of stationarity, the dynamics of delay selection at a single cell and the coordination of synaptic development along the afferent fibre separate,

Correspondence to: J.L. van Hemmen
(e-mail: lvh@ph.tum.de)

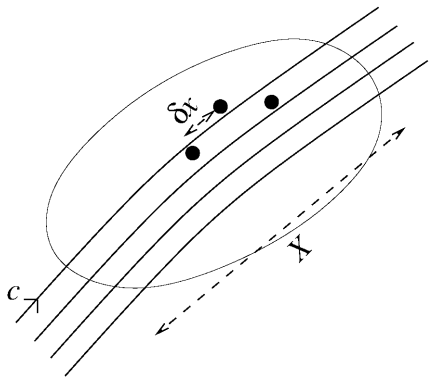

Fig. 1. Neurons (*black circles*) with average distance δx are contacted by synapses from axons (*solid lines*) that cross an area of length X in a predominant direction. Afferent activity is conducted at velocity c

which yields a quantitative estimate of the strength of AMSL (Sect. 5). We also obtain a theoretical prediction of the time course of order parameters measuring the extent of delay selection both at a single cell and within the distribution of edge delays (Sect. 6). The result of delay selection is a restriction of edge delays to a small interval. As a consequence, afferent activity is temporally precisely translated to postsynaptic excitation (Sect. 7).

An example of a delay-line topology is the model of Jeffress (1948) for neuronal detection of interaural time differences (ITDs). Section 8 shows how the introduced framework applies to the development of the laminar nucleus in barn owls, forming a map of the bird's surrounding azimuthal space (Leibold et al. 200l).

2 Homosynaptic learning

Delay selection through synaptic plasticity at the level of a single neuron is described by a learning rule for the efficacies J_{mn} of synapses between the nth afferent axon and the mth postsynaptic neuron. The $1 \le n \le N$ synapses are providing their input at times t_n^f. The firing times of the postsynaptic neurons are denoted by t_m^f. Given the firing times, the change $\Delta J_{mn}(t) := J_{mn}(t) - J_{mn}(t-\mathscr{T})$ of the efficacy of synapse m during a learning session of duration $\mathscr{T}$ and ending at time t is governed by several factors:

$$\Delta J_{mn}(t) = \eta \Bigg[\sum_{t-\mathscr{T} \le t_n^f < t} w^{\text{in}} + \sum_{t-\mathscr{T} \le t_m^f < t} w^{\text{out}} + \sum_{t-\mathscr{T} \le t_n^f, t^n < t} W(t_n^f - t_m^f) \Bigg] . \tag{1}$$

Here the firing times t_m^f of the postsynaptic neuron may, and in general will, depend on J_{mn}. We now focus on the individual terms. The prefactor $0 < \eta \ll 1$ reminds us explicitly of learning being slow on a neuronal time scale. Throughout what follows we refer to this condition as the *adiabatic hypothesis*. It has been shown to hold in numerous biological situations and has been a mainstay of computational neuroscience ever since. It may also play a beneficial role in an applied context. If it does not hold, a numerical implementation of the learning rule (1) is straightforward, but an analytical treatment is not.

Each incoming spike and each action potential of the postsynaptic neuron change the synaptic efficacy by ηw^{in} and ηw^{out}, respectively.

The last term in (1) represents the *learning window* W, which indicates the synaptic change in dependence upon the time difference $s = t_n^f - t_m^f$ between an incoming spike t_n^f and an outgoing spike t_m^f. When (e.g., for an excitatory cortical synapse) the former precedes the latter, we have $s < 0 \Leftrightarrow t_n^f < t_m^f$, and the result is $W(s) > 0$, implying potentiation. On the other hand, if the incoming spike comes "too late," then $s > 0$ and $W(s) < 0$, implying depression; see Fig. 2 and, for experimental evidence, Bi and Poo (1998) and Zhang et al. (1998).

Spike generation is (nearly) always a *local* process in time, and so are the $1 \le n \le N$ input processes generating the input spikes t_n^f. For the latter category we can, and will, take inhomogeneous Poisson processes (Kempter et al. 1998), with rate function $p_n^{\text{in}}(t)$; any other local process with independent increments or short-range correlations would do as well.

The time interval $[t-\mathscr{T}, t)$ is taken to be big since, due to the adiabatic hypothesis, learning is so slow that we can safely assume $\mathscr{T}$ to greatly exceed neuronal times such as interspike intervals and the width of the learning window. Nevertheless, we will arrive at a relatively small change of the J_{mn} values so that the assumption concerning $\mathscr{T}$ is self-consistent (otherwise we do not see anything). We can divide the time interval $[t-\mathscr{T}, t)$ into many small intervals that are, stochastically, independent of each other – apart from a minuscule overlap at their borders. Hence the sum (1) is self-averaging.

The above averaging was performed over the randomness; we now perform another one over time. To fully appreciate what is going to happen, we first turn to the differential equation

$$\frac{\mathrm{d}}{\mathrm{d}t} x = \eta F(x,t) \tag{2}$$

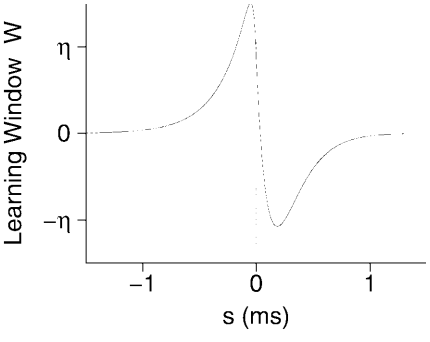

Fig. 2. The learning window W is a function of the time difference s between the pre- and the postsynaptic spike. For a generic excitatory synapse we have $W(s) > 0$ for $s < 0$ and $W(s) < 0$ for $s > 0$. Parameters have been taken from Kempter et al. (2001)

where η is "small" and $F(x,t)$ for fixed x is a periodic function of t, i.e, $F(x,t+\mathscr{T}) = F(x,t)$. After one period x has hardly changed so that, *for fixed* x, we can average F over t. That is to say, instead of (2) one studies (Sanders and Verhulst 1985; Verhulst 1986)

$$\bar{F}(x) := \frac{1}{\mathscr{T}} \int_{t-\mathscr{T}}^{t} \mathrm{d}t' F(x,t') \quad \Rightarrow \quad \frac{\mathrm{d}}{\mathrm{d}t} x = \eta \bar{F}(x) \ . \tag{3}$$

Here the integral over time, viz., t', is performed *with* x, the argument of $\bar{F}$, *fixed*; the integration boundaries $t-\mathscr{T}$ and t of the integral in (3) can be replaced by 0 and T, respectively. Hence the differential equation we arrive at is an autonomous one since $\bar{F}$ does not depend explicitly on t. It is plain that the whole argument hinges on η *being small*. In fact, under suitable conditions the 'method of averaging' (Sanders and Verhulst 1985; Verhulst 1986) can be generalized to nonperiodic F. Here we will simply average over a period of duration $\mathscr{T}$ and often use an overbar to indicate this.

We now return to our problem, viz., (1) averaged over the randomness, and average over time as well. This sounds quite harmless (it is) but we will soon see the effect is beneficial. To simplify the notation, we first introduce two spike flows,

$$S_n(t) = \sum_{t_i^f \le t} \delta(t - t_n^f), \quad S_m(t) = \sum_{t_m^f \le t} \delta(t - t_m^f) \ , \tag{4}$$

and rewrite (1), introducing angular brackets to indicate an average over the randomness:

$$\frac{\Delta J_{mn}(t)}{\mathscr{T}} = \eta \left\{ \frac{1}{\mathscr{T}} \int_{t-\mathscr{T}}^{t} \mathrm{d}t' [w^{\mathrm{in}} \langle S_n(t') \rangle + w^{\mathrm{out}} \langle S_m(t') \rangle] + \frac{1}{\mathscr{T}} \int_{t-\mathscr{T}}^{t} \mathrm{d}t' \int_{t-\mathscr{T}-t'}^{t-t'} \mathrm{d}s W(s) \, \langle S_n(t'+s) S_m(t') \rangle \right\} . \tag{5}$$

It is evident that both types of averaging – over randomness and over time – have been taken into account. So far so good. The first term on the right-hand side of (5), the time average $\overline{\langle S_n(t) \rangle}$ of the rate function $\langle S_n(t') \rangle$ for times t' in the interval $[t-\mathscr{T}, t)$, is a mean which we call $\nu_n^{\mathrm{in}}(t)$. For an inhomogeneous Poisson process this is nothing but the mean intensity $p_n^{\mathrm{in}}(t)$, where the probability of finding one spike in an interval of length Δt near t is $p_n^{\mathrm{in}}(t)\Delta t$. The second term, the time average of $\langle S_m(t) \rangle$, which is to be called $\nu_m^{\mathrm{out}}(t)$, is harder to compute since it entails both the outgoing and all the incoming processes, the latter "deciding" together when an action potential will be generated. For later reference we summarize the above two definitions:

$$\nu_n^{\mathrm{in}}(t) := \overline{\langle S_n(t') \rangle}, \qquad \nu_m^{\mathrm{out}}(t) := \overline{\langle S_m(t) \rangle} \ . \tag{6}$$

The former refers to the input only, the latter takes the output by itself.

The double integral in (5) is explicitly correlating input and output, a distinguishing property of Hebbian learning. Let us take a "typical" t', say $t' = t - \mathscr{T} + x\mathscr{T}$ with $0 < x < 1$. Then the lower bound of the integral over s is effectively $-x\mathscr{T}$, while the upper bound is $(1-x)\mathscr{T}$. The learning window W is something *local in time* – much, much shorter than $\mathscr{T}$. Hence for our "typical" t' the lower bound of the integral over s is $-\infty$ whereas the upper bound is $+\infty$ so that, up to a negligible error, we are left with

$$\frac{1}{\mathscr{T}} \int_{t-\mathscr{T}}^{t} \mathrm{d}t' \int_{-\infty}^{\infty} \mathrm{d}s W(s) \langle S_n(t'+s) S_m(t') \rangle = \int_{-\infty}^{\infty} \mathrm{d}s W(s) \frac{1}{\mathscr{T}} \int_{t-\mathscr{T}}^{t} \mathrm{d}t' \langle S_n(t'+s) S_m(t') \rangle \ . \tag{7}$$

Returning to (5), we note that we can transform it into a differential equation since $\Delta J_{mn}(t) = J_{mn}(t) - J_{mn}(t-\mathscr{T})$ and, due to the adiabatic hypothesis, the change of J_{mn} is so slow that $\Delta J_{mn}(t)/\mathscr{T}$ can be replaced by $\mathrm{d}J_{mn}/\mathrm{d}t$. In other words, we choose $\mathscr{T}$ so large that it greatly exceeds all neuronal times, e.g., interspike intervals and the width of the learning window W, but on the other hand is much smaller than $(\eta\nu)^{-1}$ for occurring firing rates ν – all in all, a condition fully consistent with the Hebbian philosophy of "practice makes perfect." That is to say, $\mathscr{T}$ separates neuronal and learning time scales. Then we find, using (5)–(7), that

$$\frac{\mathrm{d}}{\mathrm{d}t} J_{mn} = \eta \Big[w^{\mathrm{in}} \nu_n^{\mathrm{in}} + w^{\mathrm{out}} \nu_m^{\mathrm{out}} + \int_{-\infty}^{\infty} \mathrm{d}s W(s) \frac{1}{\mathscr{T}} \int_{t-\mathscr{T}}^{t} \mathrm{d}t' \langle S_n(t'+s) S_m(t') \rangle \Big] \ . \tag{8}$$

This equation is exact and describes the time evolution of *infinitesimal* synaptic plasticity, as we call it, for a neuron with given inputs.

A nice aspect of (8) is that the final integral over t' is nothing but the time-averaged correlation function. The correlation function itself is $\langle S_n(t'') S_m(t') \rangle$. We may interpret it as the joint probability density for observing an input spike at synapse n at the time t'' and an output spike of cell m at time t'. Hence we write

$$C_{mn}(t, t+s) := \frac{1}{\mathscr{T}} \int_{t-\mathscr{T}}^{t} \mathrm{d}t' \langle S_n(t'+s) S_m(t') \rangle = \overline{\langle S_n(t+s) S_m(t) \rangle} \ , \tag{9}$$

the second equality being just a definition. Altogether we get a synaptic dynamics of appealing simplicity (Kempter et al. 1999; van Hemmen 2000):

$$\left(\frac{\mathrm{d}}{\mathrm{d}t} J_{mn} \right)_{\mathrm{local}} = \eta \Big[w^{\mathrm{in}} \nu_n^{\mathrm{in}} + w^{\mathrm{out}} \nu_m^{\mathrm{out}} + \int \mathrm{d}s W(s) C_{mn}(t, t+s-\Delta_{mn}) \Big] \ . \tag{10}$$

In this form the learning equation is easy to remember: the input rate ν_n^{in} modifies the synaptic efficacy through w^{in}, the output rate ν_m^{out} does so through w^{out}, and the Hebbian correlation function C_{mn} favors or disfavors it through the learning window W.

Appearances are deceiving, however. Not only do ν_m^{out} and C_{mn} depend on J_{mn} but also, through S_m, on all the

other $J_{mn'}$ with $n' \neq n$. Moreover, neuronal firing is intrinsically nonlinear. Hence synaptic dynamics is an intricate collective process.

Conclusion

The generic form of W, i.e., $W(s) < 0$ for positive s and $W(s) > 0$ for negative s (see Fig. 2), implies that presynaptic spikes from axon n arriving at cell m after a postsynaptic action potential ($s > 0$) lead to a decrease of the efficacy J_{mn}, whereas the arrival of presynaptic firing before an action potential at m ($s > 0$) yields an increase of J_{mn}. Synaptic connections incidently giving rise to a postsynaptic spike are strengthened, thus having a slight advantage in firing the postsynaptic cell again, and so on; whereas, on average, the other synapses are depressed. This mechanism can be regarded as a self-organizing development of the synaptic delay structure in order to optimize the sensitivity of postsynaptic firing to temporally coherent presynaptic signals.

3 Axon-mediated synaptic learning

Let us define a *map* as a neuronal representation of the sensory world or aspects thereof, such as time. By its very definition, *many* neurons are involved in constituting a map.

In Sect. 2 we have seen how the *collective* dynamics of synaptic development at each specific neuron is governed by the synapses' learning window, despite the fact that the latter is operating locally in space, viz., at a synapse, and in time, as in Fig. 2 where its temporal width is 1 ms. The idea behind this collective behavior is that the synapses together "decide" whether or not the neuron they are attached to will fire. Consequently a neuron's temporal accuracy may greatly improve but there is no reason why it should join a map as a neuronal representation of the sensory surroundings, here of its temporal aspects (cf. Figs. 1 and 7a). To this end, synapses at *different* neurons have to interact. We will now analyze such an interaction (i.e., AMSL).

The abstract concept of delay selection at the level of afferent fibers comes along with the introduction of the so-called *axonal weight* K_n. It is defined as the sum of all synaptic efficacies of axon n:

$$K_n = \sum_m J_{mn} \quad . \tag{11}$$

A stable configuration of axonal weights in a delay-line regime requires that few axons with similar edge delay Δ_{0n} provide a high value of K_n, whereas all the others are near 0 and, hence, degenerate. A coordinated development of synaptic efficacies at different postsynaptic cells that fits into this concept is realized through a dynamics of the synaptic weights J_{mn} in such a way that neuronal activity at one synapse induces alterations of all synapses at the same axon. Formally we write

$$\frac{\mathrm{d}}{\mathrm{d}t} J_{mn} = \sum_{m' \text{ at axon } n} \left[\delta_{mm'} \left(\frac{\mathrm{d}}{\mathrm{d}t} \right)_{\text{local}} + \rho_{mm'} \left(\frac{\mathrm{d}}{\mathrm{d}t} \right)_{\text{AMSL}} \right] J_{m'n} \quad , \tag{12}$$

where $\left(\frac{\mathrm{d}}{\mathrm{d}t}\right)_{\text{local}}$ is given by (10), and

$$\left(\frac{\mathrm{d}}{\mathrm{d}t} J_{mn} \right)_{\text{AMSL}} = \eta \left[u^{\text{in}} v_n^{\text{in}} + u^{\text{out}} v_m^{\text{out}} + \int \mathrm{d}s U(s) C_{mn}(t, t + s - \Delta_{mn}) \right] \tag{13}$$

describes axonally propagated synaptic changes. The quantities u^{in}, u^{out}, and $U(s)$ may differ from those in the homosynaptic dynamics (10), but are assumed to be of the same order of magnitude.

In summary, besides alterations $\left(\frac{\mathrm{d}}{\mathrm{d}t} J_{mn}\right)_{\text{local}}$ initiated locally, there is also a contribution $\left(\frac{\mathrm{d}}{\mathrm{d}t} J_{mn}\right)_{\text{AMSL}}$ that stems from the change of synaptic efficacies at neighboring cells contacting the same afferent fiber n and mediated by the axon through a coupling matrix $\rho_{mm'}$ (Fig. 3).

Hence the latter is called AMSL. Its spatial dependence and strength are determined by the matrix $\rho_{mm'}$, which – for the sake of convenience – is assumed to be translationally invariant, i.e., $\rho_{mm'} = \rho_{m+m_0 m'+m_0}$ for $1 < m_0 < M$ fixed, and symmetric, i.e., $\rho_{mm'} = \rho_{m'm}$. Experimental evidence for presynaptically unspecific contributions is available for various locations in the nervous system (Bonhoeffer et al. 1989; Cash et al. 1996; Fitzsimonds et al. 1997; Fitzsimonds and Poo 1998; Goda and Stevens 1998; Tao et al. 2000). The present application and the ensuing theoretical analysis is due to Kempter et al. (2001) and Leibold et al. (200l), respectively.

4 Correlation functions of Poisson neurons

The discussion of differential equations (10) and (12) requires explicit expressions for time-averaged rates ν and correlations C, both of which in general depend nonlinearly on the 'weight vector' J_{mn}. To this end we assume from now on that pre- as well as postsynaptic

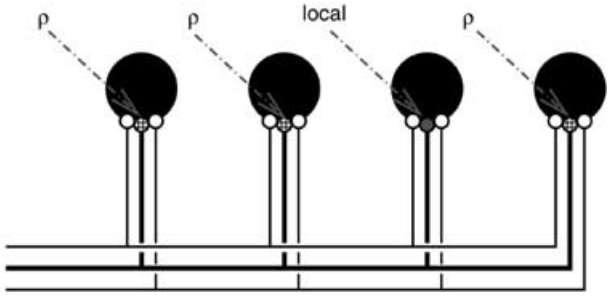

Fig. 3. Local weight changes (at the *gray* synapse of the third cell on the left) are presynaptically propagated (along the *thick line*) to synapses (*checkered circles*) at neighboring neurons, and weighted through matrix elements $\rho_{mm'}$

spike generation results from inhomogeneous poissonian processes (van Hemmen 2000), where afferent activity is modeled through given intensities $p_n^{\text{in}}(t)$. This means the following. We write $p(t) := p_n^{\text{in}}(t)$ as shorthand and define an inhomogeneous poissonian process by three properties: (i) the probability of getting a *single* event during the interval $[t, t+\Delta t)$ with $\Delta t \to 0$ is $p(t)\Delta t$, (ii) the probability of getting two or more events is $o(\Delta t)$, and (iii) events in disjoint intervals are independent.

Postsynaptic firing is due to rates $p_m^{\text{out}}(t) = p_{\text{F}}[v_m(t)]$, with p_{F} being an analytic function – called the gain function – of the instantaneous membrane potential of the mth neuron:

$$\begin{aligned} v_m(t) &= \sum_{n=1}^{N} J_{mn} \sum_{\{t_n^f\}} \epsilon(t - t_n^f - \Delta_{mn}) \\ &= \sum_{n=1}^{N} J_{mn} \int \mathrm{d}s \epsilon(s) S_n(t - s - \Delta_{mn}) \ . \end{aligned} \tag{14}$$

As above, $\{t_n^f\}$ labels the set of presynaptic firing times of fiber n, and $\epsilon(s)$ is an excitatory postsynaptic potential (EPSP) model, which is positive, causal, and normalized, i.e., $\int_0^\infty \mathrm{d}s\epsilon(s) = 1$ (Fig. 4).

4.1 Stationary input

We assume temporally averaged rates and correlations of the input processes to be invariant in time, a property that we call *stationarity on time scale* $\mathscr{T}$. Rates are therefore simply numbers $\nu_n^{\text{in}}(t) = \nu_n^{\text{in}}$, and correlation functions only depend upon time differences $C_{nn'}(t,t') = C_{nn'}(t-t')$. This will be the central hypothesis that allows separation of the synaptic dynamics at the single-cell level and the selection of delay lines through AMSL (see Sect. 5).

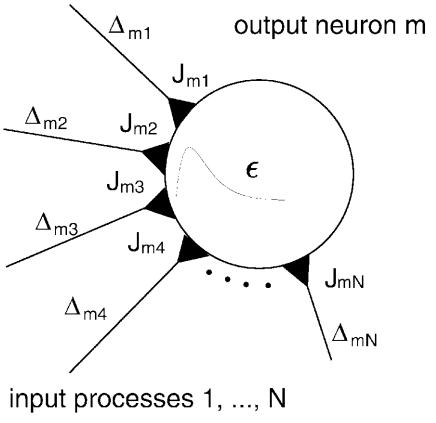

Fig. 4. Model of synaptic transmission. Once neuron n fires it takes an axonal deay Δ_{mn} before the spike reaches neuron m. Each of the N synapses connecting to output neuron m is described by a single variable J_{mn}, its efficacy or strength. Its effect is to adjust the amplitude of the corresponding spike-response kernel ϵ. The sum of all responses yields the postsynaptic membrane potential $v_m(t)$ given by (14)

4.2 Postsynaptic firing rates

Correlation functions $\langle S_m(t)S_n(t+r)\rangle$ can be derived from rates $\langle S_m(t)\rangle = \langle p_m^{\text{out}}(t)\rangle = \langle p_{\text{F}}[v_m(t)]\rangle$ using Bayes' formula (Kempter et al. 1998; Leibold et al. 2002), which is nothing but an expression for conditional probabilities (Ash 1972):

$$\langle S_m(t)S_n(t+r)\rangle = \langle S_m(t)|n, t+r\rangle p_n^{\text{in}}(t+r) \ ,$$

where $\langle S_m(t)|n,t'\rangle$ labels the average rate at cell m under the condition of a presynaptic spike in fiber n at time t'. We now calculate the postsynaptic intensities $\langle S_m(t)\rangle = \langle p_{\text{F}}[v_m(t)]\rangle$. The average on the left-hand side of the above equation is over both pre- and postsynaptic firing, whereas the right-hand average is meant presynaptically only.

Since we have chosen the gain function p_{F} to be analytical, we can write

$$p_{\text{F}}(v) = \sum_k f^{(k)} v^k \ ,$$

with finite $f^{(k)} \in \mathbb{R}$ and $\lim_{k\to\infty} f^{(k)} v^k = 0$. Then the time-averaged rates can be written as

$$\begin{aligned} \overline{\langle p_{\text{F}}[v_m(t)]\rangle} &= \sum_k f^{(k)} \overline{\langle [v_m(t)]^k \rangle} \\ &= \sum_k f^{(k)} \left[\prod_{j=1}^{k} \sum_{n_j} J_{mn_j} \int \mathrm{d}s_j \epsilon(s_j) \right] \\ &\quad \times \overline{\left\langle \prod_{j=1}^{k} S_j(t - \Delta_{mn_j} - s_j) \right\rangle} \ . \end{aligned} \tag{15}$$

Input activity has been assumed to be stationary on timescale $\mathscr{T}$ and, as a consequence, the time-averaged multispike correlation in (15) is a function of the $k-1$ differences of its k arguments only. It is thus independent of the time t, as is $\nu_m^{\text{out}} = \overline{\langle p_{\text{F}}[v_m(t)]\rangle}$. The latter then solely depends upon the set of delay differences $\{\Delta_{m1} - \Delta_{m2}, \ldots, \Delta_{mN-1} - \Delta_{mN}\}$.

Calculating the conditional averages we obtain

$$\langle p_{\text{F}}[v_m(t)]|n, t+r\rangle = \sum_k f^{(k)} \langle [v_m(t)]^k | n, t+r\rangle \ , \tag{16}$$

and hence

$$\begin{aligned} \langle S_m(t)S_n(t+r)\rangle &= \langle p_{\text{F}}[v_m(t)]|n,t+r\rangle p_n^{\text{in}}(t+r) \\ &= \sum_k f^{(k)} \langle [v_m(t)]^k | n, t+r\rangle p_n^{\text{in}}(t+r) \\ &= \sum_k f^{(k)} \langle [v_m(t)]^k S_n(t+r)\rangle \ . \end{aligned} \tag{17}$$

Inserting (14) into (17) and considering stationarity, we find that also the time average of (17) only depends on delay differences and $(r - \Delta_{mn_j})$. Since in (10) and (13) the time difference r equals $r = s - \Delta_{mn}$, (12) only depends on the set of delay differences $\{\Delta_{mn_i} - \Delta_{mn_j} | i < j\}$, so that the learning equation (12) is *autonomous*.

4.3 Formulae for exponential gain function

In the case of an exponential gain function

$$p_{\mathrm{F}}(v) = v_0 \exp[\beta v] \ ,$$

the above calculations with $f^{(k)} = v_0 \beta^k / k!$ yield an explicit form of rate and correlation (Leibold et al. 2002), viz.,

$$\langle p_{\mathrm{F}}[v_m(t)] \rangle = v_0 \exp\left\{ \sum_{n=1}^{N} \int_0^\infty \mathrm{d}s \; p_n^{\mathrm{in}}(t - s - \Delta_{mn}) \times \left[e^{\beta J_{mn} \epsilon(s)} - 1 \right] \right\} \tag{18}$$

and

$$\langle S_m(t) S_n(t+r) \rangle = \langle p_{\mathrm{F}}[v_m(t)] \rangle p_n^{\mathrm{in}}(t+r) \times \exp[\beta J_{mn} \epsilon(-r - \Delta_{mn})] \ . \tag{19}$$

Both will be useful for treating the example in Sect. 8.

5 Separability of the linear approximation

In general, one can find no explicit solution to the highly nonlinear differential equation (12). We thus turn towards the analysis of the linearized dynamics in the vicinity of an appropriate fixed point $J_{mn} = J_{mn}^{\mathrm{fix}}$.

To this end, we define a parameter regime to be *biologically relevant* if the learning equation (12) provides a fixed point with $J_{mn}^{\mathrm{fix}} > 0$, positive rate $\overline{\langle p_{\mathrm{F}}[v_m(t)] \rangle}$, and a domain of attraction that includes the generic initial conditions. We already know that (12) is autonomous and solely dependent on the set of delay differences $\{\Delta_{mn_i} - \Delta_{mn_j} | i < j\}$. The same therefore applies to a linearized dynamics for the deviations $\imath_{mn} \equiv J_{mn} - J_{mn}^{\mathrm{fix}}$ from a biologically relevant fixed point. In other words, we discuss the linear dynamics

$$\frac{\mathrm{d}}{\mathrm{d}t} \imath_{mn} = \sum_{m' \text{at axon } n} \sum_{n'} \left[(L_{\mathrm{local}})_{nn'} \delta_{mm'} + (L_{\mathrm{AMSL}})_{nn'} \rho_{mm'} \right] \imath_{m'n'} \tag{20}$$

where $(L_\star)_{nn'} = L_\star(\Delta_{mn} - \Delta_{mn'}) = L_\star(\Delta_{0n} - \Delta_{0n'})$ and $\star =$ "local" or "AMSL". The last equality is due to $\Delta_{mn} = \Delta_{0n} + x(m)/c$, which resembles a delay-line topology. The spatial position $x(m)$ of the postsynaptic neurons is often modeled as $x(m) = m\delta x$, corresponding to equidistant cells. Analogously, assuming a large number $N > 100$ of afferents, we model the edge delays as

$$\Delta_{0n} = n\Lambda / N \ .$$

The parameter Λ thereby denotes the width of available delays. The last step has an important implication, viz., the matrices $(L_\circ)_{nn'}$ become cyclic, i.e., $(L_\circ)_{nn'} = (L_\circ)_{n-n'}$. Consequently both L_{local} and L_{AMSL} are diagonalized by the same orthonormal set of eigenvectors ϕ_n , viz., plane waves

$$\phi_n(\mu) = \frac{1}{\sqrt{N}} \exp\left(\frac{2\pi i \mu n}{N} \right) , -\frac{N}{2} < \mu \leq \frac{N}{2} \ . \tag{21}$$

The eigenvalues $\lambda_\star(\mu)$ of $L_\star$ are then obtained as

$$\sum_{nn'} \phi_n^*(\mu) (L_\star)_{nn'} \phi_{n'}(\mu) = \lambda_\star(\mu) \ .$$

As an important consequence we note that the eigenvectors of the linear operator in (20) separate into a subcollection ϕ_n that describes synaptic plasticity at a single neuron, and another subcollection ψ_m that explains the coordination of delay selection along the axons. The eigenvectors Φ_{mn} of the complete dynamics (20) are thus products

$$\Phi_{mn}(l, \mu) = \psi_m(l, \mu) \phi_n(\mu) \ , \tag{22}$$

where the ψ_m comply with

$$\sum_{m'} [\delta_{mm'} \lambda_{\mathrm{local}}(\mu) + \rho_{mm'} \lambda_{\mathrm{AMSL}}(\mu)] \psi_{m'}(l, \mu) = \lambda(l, \mu) \psi_m(l, \mu) \ . \tag{23}$$

We now return to the properties of the axonal interaction matrix $\rho_{mm'}$. It was supposed to be symmetric and translationally invariant, i.e., cyclic. As a result the ψ_m are also plane waves:

$$\psi_m(l, \mu) \equiv \psi_m(l) = \frac{\exp(2\pi i l m / M)}{\sqrt{M}} \tag{24}$$

and the eigenvalues belonging to (23) read

$$\lambda(l, \mu) = \lambda_{\mathrm{local}}(\mu) + M \hat{\rho}_l \lambda_{\mathrm{AMSL}}(\mu) \tag{25}$$

where

$$\hat{\rho}_l = \sum_{m=-M/2}^{M/2} \rho_{m0} e^{-2\pi i l m / M}$$

denotes the spatial Fourier transform of the coupling matrix. This only holds exactly for $M \to \infty$ or periodic boundary conditions, but as shown by Ledermann (1944), for finite M the alignment of the spectrum remains unchanged. Since we have assumed symmetric axonal coupling, $\hat{\rho}(l)$ is simply a real number. In the special case $\rho_{mm'} = \rho =$constant, however (25) is exact for all M and the eigenvalues are

$$\lambda(l, \mu) = \lambda_{\mathrm{local}}(\mu) + M\rho \ \delta_{l0} \lambda_{\mathrm{AMSL}}(\mu) \ .$$

Conclusions

Since the axonal interaction contributes to the eigenvalue with ρM, and $\lambda_{\mathrm{AMSL}}(\mu)$ is of the same order of magnitude as $\lambda_{\mathrm{local}}(\mu)$, a relatively small value of $\rho \approx 1/M$ already has a noticeable effect on the synaptic dynamics.

The selection of edge delays, i.e, of whole axonal arbors, requires that all synapses at an axon should be altered similarly: if one synapse is strengthened all synapses at the same axon ought to be strengthened, and if

one is depressed all of them ought to be depressed. The only eigenvector $\psi_m(l)$ that is in agreement with the above picture is the one for which $l = 0$. The strength of the coordinating effect is then represented by the eigenvalue $\lambda(0,\mu) = \lambda_{\text{local}}(\mu) + M\rho\lambda_{\text{AMSL}}(\mu)$. It exceeds eigenvalues for which $l \neq 0$, if $M\rho > 1$; it then dominates the synaptic dynamics and leads to a synchronized development along the axonal arbors.

6 Structure indices

The status of delay selection at the single-cell and axonal levels can be quantified through so-called *structure indices*. We define them as projections of the weight deviations ι_{mn} onto eigenvectors of the linearized dynamics.

1. The so-called *axonal structure index* V^{axon} is the projection of ι_{mn} onto the eigenvector $\Phi_{mn}(0,\mu)$ that describes the synchronization of synaptic dynamics along the axonal arbors:

$$V^{\text{axon}} = \frac{1}{\sqrt{MN}} \left| \sum_{mn} \iota_{mn} \Phi_{mn}(0,\mu) \right| \ . \tag{26}$$

2. In contrast, the *average structure index* V^{avg} is generated by the projections of ι_{mn} onto $\phi_n(\mu)$, averaged over all postsynaptic cells:

$$V^{\text{avg}} = \sqrt{\frac{1}{MN} \sum_{m} \left| \sum_{n} \iota_{mn} \phi_n(\mu) \right|^2} \ . \tag{27}$$

   It measures the average extent of synaptic structure formation at single-cell level and therefore serves as an upper bound for V^{axon} (see Eq. 31).

In order to calculate the time course of both indices, we expand ι_{mn} in eigenvectors Φ_{mn}:

$$\iota_{mn} = \sum_{l\mu} a(l,\mu) \Phi_{mn}(l,\mu) \ .$$

Since

$$a(l,\mu)(t) = \exp[t\lambda(l,\mu)] a(l,\mu)(0)$$

and the eigenvectors are orthonormal, we find

$$V^{\text{axon}}(t) = \frac{1}{\sqrt{MN}} \left| a(0,\mu)(0) e^{\lambda(0,1)t} \right|$$

and

$$V^{\text{avg}}(t) = \sqrt{(MN)^{-1} \sum_{l} \left| a(l,\mu)(0) e^{\lambda(l,1)t} \right|^2} \ .$$

For the sake of simplicity we assume the axonal coupling matrix to be of the form $\rho_{mm'} = \rho$ for all m, m' and $\Re\{\lambda_{\text{local}}(\mu)\} = \Re\{\lambda_{\text{AMSL}}(\mu)\} =: \lambda^T$. The eigenvalues thus have real parts $\Re\{\lambda(l,1)\} = \lambda^T(1 + \rho M \delta_{l0})$. We obtain

$$V^{\text{axon}}(t) = \gamma_0 e^{t\lambda^T(1+\rho M)} \tag{28}$$

and

$$V^{\text{avg}}(t) = \gamma_0 e^{t\lambda^T(1+\rho M)} \times \left[1 + (M-1) \left(\frac{\gamma_1}{\gamma_0} \right)^2 e^{-2\rho M t \lambda^T} \right]^{1/2} \ , \tag{29}$$

where

$$\gamma_0 := \frac{|a(0,\mu)(0)|}{\sqrt{MN}} \ , \tag{30}$$

$$\gamma_1 := \sqrt{(MN)^{-1} \sum_{l;l\neq 0} \frac{|a(l,\mu)(0)|^2}{(M-1)}} \ .$$

In (28) and (29) the initial values $a(l,\mu)(0)$ are reduced to the two numbers γ_0 and γ_1. To estimate their order of magnitude, we calculate expectation values. As initial conditions we assume $\iota_{mn}(0) = \xi_{mn}$, with ξ_{mn} being uncorrelated white noise with mean zero and correlation

$$\langle \xi_{mn} \xi_{m'n'} \rangle = d^2 \delta_{mm'} \delta_{nn'} \ .$$

We end up with

$$\gamma_0 \approx \gamma_1 \approx \frac{d}{\sqrt{MN}} \ .$$

These approximations are used for plotting the time evolution of the order parameters, viz., (28) and (29), in Fig. 5 for the set of parameters used by Kempter et al. (2001).

Figures 5 and 6 show that the theoretical predictions are a reasonable approximation of the data obtained by numerical simulations with the same set of parameters.

Global order is always less than local order since

$$\frac{V^{\text{axon}}(t)}{V^{\text{avg}}(t)} = \left[1 + \frac{(M-1)(\gamma_1/\gamma_0)^2}{e^{2\rho M t \lambda^T}} \right]^{-1/2} < 1 \tag{31}$$

while $M > 1$. As $t \to \infty$, the ratio of vector strengths in (31) approaches 1 if both ρ and λ^T are positive. So, if we wait sufficiently long, we will gain a perfect, globally ordered map. The final quality of the map therefore seems to have only a little dependence upon ρ. These considerations, however, only hold if the dynamics remains linear. For biological systems this assumption is in general not fulfilled, as the resources available for synaptic modification are restricted. This restriction can be mimicked by introducing an upper bound for the local order parameter V^{avg}. Once the boundary is reached (at $t = t^{\text{freeze}} > 0$), the whole dynamics is assumed to be frozen. The difference between local and global order at freezing time, however, has a strong dependence upon ρ (Fig. 5).

For fixed $t = t^{\text{freeze}} > 0$, (31) shows that the bigger the axonal coupling ρ, the more the difference between the values of both order parameters diminishes. So one could argue that map formation becomes more effective with larger axonal coupling strength. In Leibold et al. (2002) it is shown that this is not the case and that, due to noise, the upper limit for the axonal coupling strength is of the order $\rho \gtrsim \mathcal{O}(M^{-1/2})$.

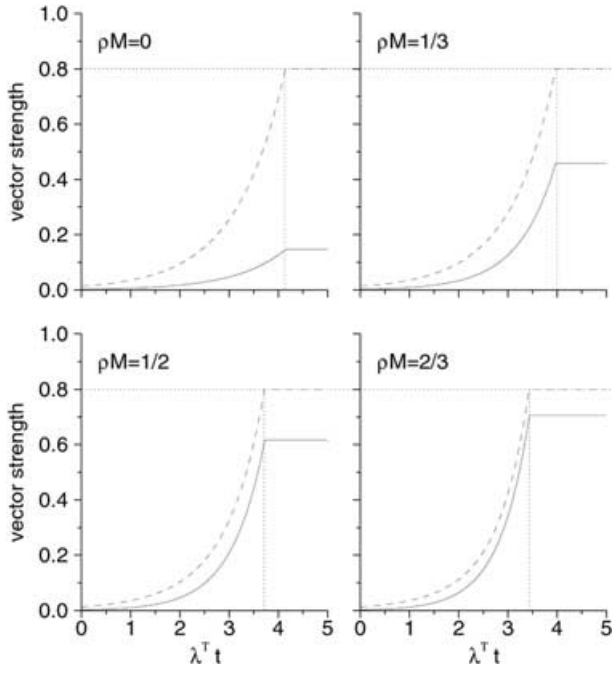

Fig. 5. Dynamics of the order parameters. The global order parameters V^{axon} (*solid lines*) and V^{avg} (*dashed lines*) are plotted as functions of time (see Eqs. 28, 29) represented by the horizontal axes. The interaction strength ρM is varied systematically from $\rho M = 0$ (no interaction) to $\rho M = 2/3$ (strong interaction). Once the local order parameter reaches a saturation threshold, say 0.8 (*dotted horizontal lines*), synapse growth stops, which can be achieved, e.g., by introducing an upper bound for the single synaptic weights. Hence at the same time (*dotted vertical lines*) also the global order parameter stops increasing. Thus the difference between global and local saturation depends on ρM. In accordance with Kempter et al. (2001), the following parameters have been used: $d = 0.2$, $N = 250$, $M = 30$

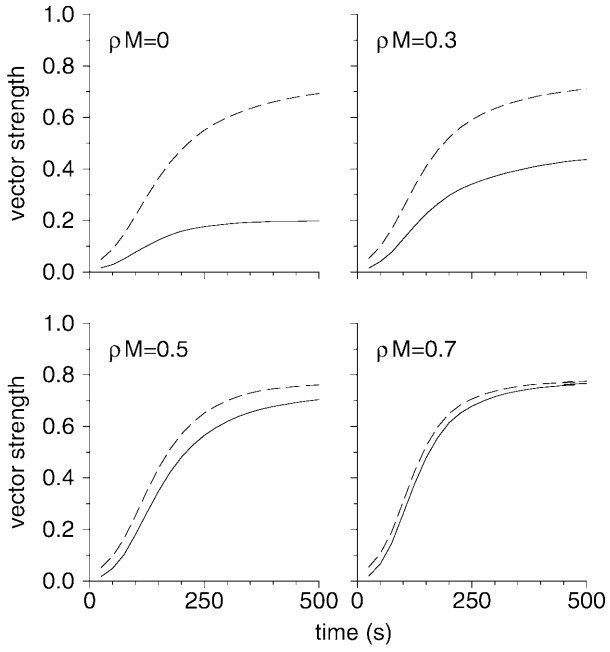

Fig. 6. Dynamical evolution of *order parameters* as given by numerical simulations. The global (*solid lines*) and local (*dashed lines*) order parameters have been plotted as functions of time (cf. Fig. 5). Other parameters have been chosen as in Kempter et al. (2001). As the interaction strength ρM is increased, the difference between the saturation values of the global and local orders diminishes. Saturation is realized by an upper bound of 2 for the individual synaptic weights

7 Traveling waves

In order to visualize the effect of the delay-line topology on postsynaptic excitation, we calculate the average membrane potential along the axonal arbor for a given synaptic configuration $J_{mn} = J_{mn}^{\text{fix}} + \Phi_{mn}(0, \mu)$ and a periodic presynaptic activity with frequency $\mu/\Lambda = \omega/(2\pi)$. We obtain a traveling wave:

$$\langle v_m(t) \rangle = v_m^{\text{fix}}(t) + v_1 \cos(\omega t + \omega/cm\delta x + \varphi) \quad .$$

Besides the dynamics at the fixed point, a Hebbian-tuned structure of edge delays is responsible for wave-like propagation of postsynaptic activity. The wavelength is thereby given by $\omega/(2\pi c)$. The phase φ is provided by a global offset of presynaptic activity. The constant v_1 incorporates membrane properties.

8 Time-difference maps

As an example of a temporal map that is generated by delay lines, we refer to the laminar nucleus of barn owls. This is the first station receiving binaural input and its cells are tuned to best ITDs as well as best frequencies. Both features are organized in maps. The tonotopy gradient roughly runs in the anterior–posterior direction, whereas the best ITD gradient has been found along the dorsoventral axis of the nucleus (Sullivan and Konishi 1986; Fig. 7a).

The biological realization of the ITD map has been shown to agree with the Jeffress hypothesis (Carr 1993). He proposed an array of coincidence-detector cells with a topology the same as that shown in Fig. 7b (we return to it in Fig. 10). If, at a specific neuron, the difference of conduction delays between the axon bundles originating from the left and right ears compensates for the acoustic time difference that occurs between both ears and is caused by the sound-source location, then the cell receives spikes that are temporally highly correlated and thus (Kempter et al. 1998) fires at a high rate. Although in the young animal each axon carries a phase-locked input, the temporal dispersion of all spikes arriving at each neuron (Carr and Konishi 1990) has a width of 1 ms, i.e., one to several periods of the frequencies involved (1–9 kHz). We now show how a delay-line architecture can evolve during maturation of the animal, and thereby specify the learning equations (10) and (13) as well as the input processes.

8.1 Model formulation

First, we specify EPSP and learning windows. Since the membrane time constants in the auditory periphery of birds are known to be extremely short (e.g., in chickens the rise times are only 200μs; Reyes et al. 1996), we assume for barn owls – being auditory specialists – a membrane rise time of 100μs (Fig. 8a) and a learning

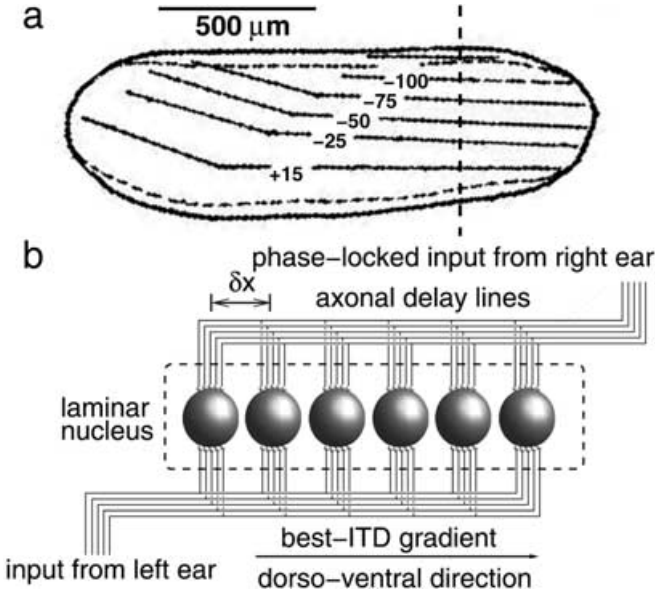

Fig. 7. **a** Interaural time difference (ITD) map in a barn owl's laminar nucleus, after Sullivan and Konishi (1986). Iso-ITD contours (*solid lines*) consist of neurons with maximal response at ITDs as indicated; e.g., −25 corresponds to the left ear leading by 25 μs. The *vertical dashed line* is the cut shown in **b**, where neuronal activity is conveyed by spike trains in axon bundles (*solid lines*) that come from the left and right ears, run in parallel to the dorsoventral direction (*arrow*), and contact neurons through synapses (*small white balls*). Measuring firing rates of neurons (*large gray spheres*) along this direction, one finds that the neuronal site where the firing rate is *maximal* varys continuously with the stimulus angle – a place code. Neurons are taken to be equidistant with $\delta x = 10\,\mu$m, a typical value

window with a temporal width that fits in this range (Fig. 8b).

Moreover, in order to minimize the number of model parameters, we set the nonlocal learning parameters equal to the local ones, i.e., $u^{\text{in/out}} = w^{\text{in/out}}$.

The spatial extent of the laminar nucleus is similar to the range of axonally mediated learning as reported by experiments (Bonhoeffer et al. 1989; Cash et al. 1996; Fitzsimonds et al. 1997). We therefore take $\rho_{mm'} = \rho$ to be constant.

The crucial step in modeling synaptic plasticity is the choice of input processes and the correlation functions that follow from them; see (10) and (13). Since the auditory system is tonotopically organized, i.e., different spectral components of the acoustic stimulus are processed at different spatial locations in the cochlear nuclei and hence in the input provided by them, cells in the laminar nucleus are exposed to afferent activity with some prevailing periodicity T_p, corresponding to the characteristic frequency $f = 1/T_\text{p}$ of the respective cochlear channel. We take this into account by defining the poissonian input rates to be periodic functions, $p^\text{in}(t) = \nu^\text{in} T_\text{p} g(t)$, where $g(t) = g(t + T_\text{p})$ with $\int_0^{T_\text{p}} \text{d}s g(s) = 1$. Any periodic function, g, can be expressed as a Fourier series:

$$g(t) = T_\text{p}^{-1} \sum_{\mu=-\infty}^{\infty} \hat{g}_\mu \exp(2\pi i \mu t / T_\text{p})$$

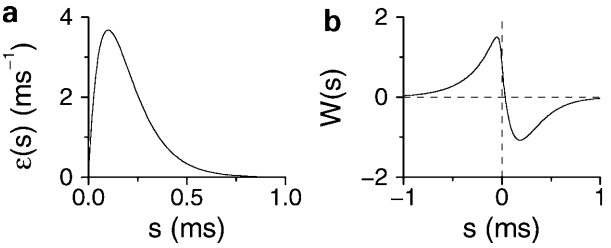

Fig. 8a,b. Excitatory postsynaptic potential $\epsilon(s) = s/\tau^2 \exp(-s/\tau)$ for $s \geq 0$, $\epsilon(s) = 0$ for $s < 0$, with $\tau = 0.1$ms **(a)** and learning window W (Kempter et al. 2001; **b**), as they have been used in the numerical simulations

with coefficients $\hat{g}_\mu = \int_0^{T_\text{p}} \text{d}s g(s) \exp(-2\pi i \mu s / T_\text{p})$. Different axons' firing densities are assumed to differ only by a retardation of delay Δ_{0n}, so that $p_n^\text{in}(t) = p^\text{in}(t - \Delta_{n0})$. We find that, by definition,

$$\overline{\langle S_n^\text{in}(t) \rangle} = \nu^\text{in}$$

and, less trivially,

$$\begin{aligned}\overline{\langle S_n^\text{in}(t) S_{n'}^\text{in}(t+r) \rangle} &= \overline{p_n^\text{in}(t) p_{n'}^\text{in}(t')} + \delta_{nn'} \delta(r) \overline{p_n^\text{in}(t)} \\ &= (\nu^\text{in})^2 \sum_\mu |\hat{g}_\mu|^2 \exp[2\pi i \mu (r + \Delta_{0n} - \Delta_{0n'})/T_\text{p}] \\ &\quad + \delta_{nn'} \delta(r) \nu^\text{in} \quad .\end{aligned}$$

Lastly, we specify the gain function p_F to be exponential (see Sect. 4.3) since we also want to cover the effect of nonlinearities on synaptic dynamics.

8.2 Fixed point

We now show that, with an exponential gain function, learning equations such as (10) have a constant, biologically relevant, fixed point $J_{mn}^\text{fix} = J^\text{fix} > 0$ under rather general conditions. We therefore insert $J_{mn} = J^\text{fix}$ into (18) and because of

$$\begin{aligned}\sum_n p^\text{in}(t - \Delta_{mn}) &= \sum_n p^\text{in}[t - x(m)/c - n T_\text{p}/N] \\ &= \nu^\text{in} T_\text{p} \sum_n g[t - x(m)/c - n T_\text{p}/N] \\ &= \nu^\text{in} \sum_{n\mu} \hat{g}_\mu e^{2\pi i \mu [t - x(m)/c - n T_\text{p}/N]/T_\text{p}} \\ &= \nu^\text{in} \sum_\mu N \delta_{\mu 0} \hat{g}_\mu = N \nu^\text{in} \underbrace{\hat{g}_0}_{1}\end{aligned}$$

the mean firing probability is constant:

$$\nu^\text{out} = \nu_0 \exp\left\{ N \nu^\text{in} \int_0^\infty \text{d}s (e^{\beta J^\text{fix} \epsilon(s)} - 1) \right\} \quad . \tag{32}$$

Consequently the correlation function in (19) is independent of t as well:

$$C_{mn}(t, t+r) = \nu^\text{out} \nu^\text{in} e^{\beta J^\text{fix} \epsilon(-r - \Delta_{mn})} \quad . \tag{33}$$

We insert (32) and (33) into (10) and obtain the fixed-point condition ($\mathrm{d}J^{\mathrm{fix}}_{mn}/\mathrm{d}t_{\mathrm{local}} = 0$):

$$\gamma := \frac{-w^{\mathrm{in}}}{v^{\mathrm{in}} \int \mathrm{d}s W^{\mathrm{eff}}(s;\beta J^{\mathrm{fix}}) + w^{\mathrm{out}}} = \frac{v^{\mathrm{out}}}{v^{\mathrm{in}}} \tag{34}$$

where the effective learning window is defined by $W^{\mathrm{eff}}(s;x) := W(s)\exp[x\epsilon(-s)]$. In biological neuronal networks the ratio γ between the input and output rates is of order 1. Any arbitrary value of $\gamma > 0$ can be obtained by adjusting w^{in} and w^{out} in (34) for any given values of v^{in} and βJ^{fix}. We thus postulate a fixed positive value γ, and due to (32) we can write

$$\frac{\ln(\gamma v^{\mathrm{in}}/v_0)}{Nv} = \int_0^\infty \mathrm{d}s[e^{\beta J^{\mathrm{fix}}\epsilon(s)} - 1] =: \psi(\beta J^{\mathrm{fix}}) \tag{35}$$

Here ψ is a monotonically increasing function of βJ^{fix} with $\psi(0) = 0$ and hence, for $\ln(\gamma v^{\mathrm{in}}/v_0) > 0$, there is a unique fixed-point solution βJ^{fix}.

8.3 Linearized synaptic dynamics

As announced in (20), for small deviations $\imath_{mn}$ the synaptic dynamics can be continously mapped upon the linear differential equation that is obtained through a Taylor expansion of (12) (Grobman-Hartman theorem, Hale and Koçak 1991; Verhulst 1996):

$$\frac{\mathrm{d}}{\mathrm{d}t}\imath_{mn} = \sum_{m'n'}\left[\frac{\partial}{\partial J_{m'n'}}\left(\frac{\mathrm{d}}{\mathrm{d}t}J_{mn}\right)\right]\Bigg|_{J_{mn}=J^{\mathrm{fix}}} \imath_{m'n'} \ .$$

The partial derivatives at the fixed point then yield the matrix $L_{nn'}$ that appears in (20):

$$L_{nn'} = \eta\beta v^{\mathrm{out}}(v^{\mathrm{in}})^2 \sum_\mu |\hat{g}_\mu|^2 \hat{W}^{\mathrm{eff}}_\mu \hat{\epsilon}^{\mathrm{eff}}_\mu e^{2\pi i\mu(\Delta_{0n}-\Delta_{0n'})/T_{\mathrm{p}}} \times \lambda^{\mathrm{post}}/N + \delta_{nn'}\lambda^{\mathrm{auto}}$$

where $\epsilon^{\mathrm{eff}}(s;x) = \epsilon(s)\exp[x\epsilon(s)]$ denotes an effective post-synaptic potential, while

$$\lambda^{\mathrm{auto}} = \eta\beta v^{\mathrm{out}} v^{\mathrm{in}} \int \mathrm{d}s\epsilon(-s) W^{\mathrm{eff}}(s;\beta J^{\mathrm{fix}})$$

and $\lambda^{\mathrm{post}} = \eta v^{\mathrm{in}} v^{\mathrm{out}} N w^{\mathrm{out}}\ \hat{\epsilon}^{\mathrm{eff}}_0$. The coefficients $\hat{W}^{\mathrm{eff}}_\mu$ and $\hat{\epsilon}^{\mathrm{eff}}_\mu$ are ordinary Fourier transforms, such as

$$\hat{W}^{\mathrm{eff}}_\mu := \int_{-\infty}^{\infty} \mathrm{d}s W^{\mathrm{eff}}(s;\beta J^{\mathrm{fix}})\exp(-2\pi i\mu s/T_{\mathrm{p}}) \ .$$

As a result, the eigenvalues of L are given by

$$\lambda(\mu) = \eta\beta v^{\mathrm{out}} N (v^{\mathrm{in}})^2 |\hat{g}_\mu|^2 \hat{W}^{\mathrm{eff}}_\mu \hat{\epsilon}^{\mathrm{eff}}_\mu + \delta_{\mu 0}\lambda^{\mathrm{post}} + \lambda^{\mathrm{auto}} \ . \tag{36}$$

Figure 9 shows $\lambda(\mu)$ as a function of $\omega = 2\pi\mu/T_{\mathrm{p}}$ for different values of βJ^{fix} and $w^{\mathrm{out}} = 0$.

For sufficiently high ω (the minimal best frequency of laminar neurons is about 1 kHz, which yields $\omega =$ 6 kHz), we find the maximal real part for μ is ± 1 and, therefore, the prominent eigenvector is $\Phi_{mn}(0,\pm 1) = \exp(2\pi i\Delta_{mn}/T_{\mathrm{p}})$, which is consistent with numerical simulations (Kempter et al. 2001) and explains experimental findings (Carr and Konishi 1990). Imaginary parts of eigenvalues of the matrix L lead to oscillations and, as such, are disadvantageous to structure formation. A closer look at Fig. 9 reveals, however, that imaginary parts are suppressed by increasing β. That is to say, nonlinearities in p_{F} can stabilize synaptic learning.

8.4 Mapping interaural time differences

After independent structure formation in both populations, the system faces two excitation waves – $v^{\mathrm{left}}_m(t)$ and $v^{\mathrm{right}}_m(t)$ – that are traveling in opposite directions; cf. Sect. 7 with $c^{\mathrm{left}} = -c^{\mathrm{right}}$. Their linear superposition leads to a standing wave:

$$\langle v^{\mathrm{left}}_m(t) + v^{\mathrm{right}}_m(t)\rangle = 2v^{(0)} + 2v^{(1)} \times \cos[\omega_{\mathrm{p}} x(m)/c + \Phi]\cos(\omega_{\mathrm{p}} t) \ . \tag{37}$$

The positions $x^{\max}$ of the interference maxima are then defined by the phase offset Φ between both classes of input processes: $x^{\max} = \mathbb{Z}cT_{\mathrm{p}}/2 - c\Phi/\omega_{\mathrm{p}}$. We have thus obtained a *place code* representing the time difference Φ/ω_{p} between both classes. The time difference is determined by both the hard-wired conduction delay between the auditory organ and the laminar cell, and by the azimuthal position of the sound source, i.e., the ITD (Fig. 10a). Since the conduction delay is an anatomic constant for each neuron, we have actually obtained a representation of the ITD in terms of position of *interference maxima* in the laminar nucleus. Because of the nonlinear gain function, these interference maxima are then transformed into firing rates, i.e., an ITD map.

9 Excursion: unreliable synapses

Although up to now spike transmission through synapses has been modeled deterministically, i.e., each

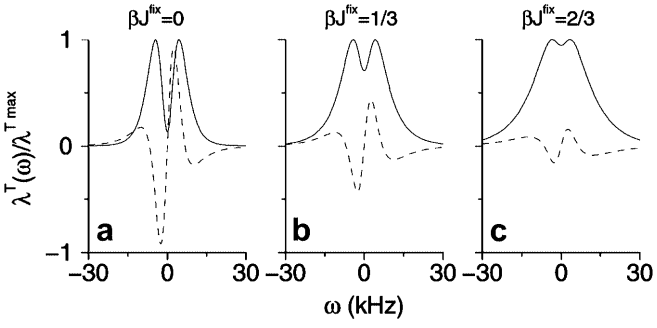

Fig. 9a–c. The normalized temporal eigenvalues $\lambda^T \propto \hat{W}^{\mathrm{eff}}\hat{\epsilon}^{\mathrm{eff}}$, for $\beta J^{\mathrm{fix}} = 0$ (**a**), 1/3 (**b**), and 2/3 (**c**), show band-pass properties. Real parts (*solid lines*) get broader as β increases, whereas imaginary parts (*dashed lines*) approach zero

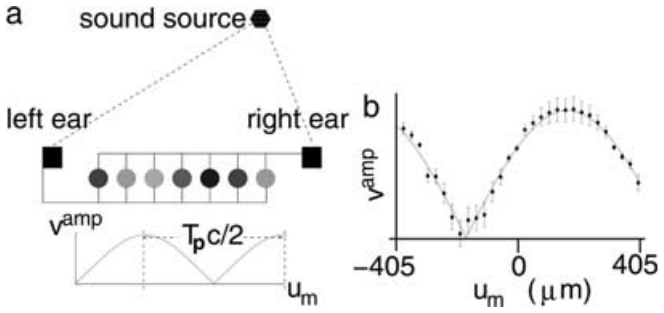

Fig. 10. a Schematic drawing of a coincidence detector (*gray circles*) array as proposed by Jeffress (1948). Acoustic stimulation is transduced to cells in the barn owl's laminar nucleus. It is delayed by (i) the spatial distance between the sound source and the ears (*dashed lines*) and (ii) the physiological transduction from the ear to the cell (*solid lines*). After delay tuning, the theoretically predicted average membrane potential $\langle v(t)\rangle$ is a standing wave across the laminar nucleus with period $T_p c/2$. Its phase is defined by the interaural time difference. The azimuthal position of the sound source in auditory space is thus mapped onto the position u_m of maximal amplitude of the membrane potential v^{amp} (the brighter the disk, the higher the amplitude of the neuron's membrane potential) within the laminar nucleus. **b** For comparison, we show the simulated amplitude of the membrane potential for an ITD of 50 μs and synaptic weights after 875 s of learning. The interaction strength is $\rho = 0.7/30$; the other parameters have been taken from Kempter et al. (2001). The amplitudes are obtained from a best fit to the time course of the standing potential wave that was averaged over 5 s. The period of v^{amp} agrees with the theoretical prediction (*solid line*)

presynaptically arriving spike safely elicits an EPSP, a more realistic description is obtained by so-called unreliable synapse models (Senn et al. 2002). The latter implies that if there is an input spike at time t and input line n, it is transmitted to the postsynaptic cell – and hence to the learning procedure – with a probability P. The mentioned procedure is equivalent to replacing the input densities p_n^{in} by $P\,p_n^{\text{in}}$. As a result, (18) and (19) read

$$\langle p_{\text{F}}^{(P)}[v_m(t)]\rangle := v_0 \exp\left\{\sum_{n=1}^{N}\int_0^\infty \mathrm{d}s P\, p_n^{\text{in}}(t-s-\Delta_{mn}) \times\left[e^{\beta J_{mn}\epsilon(s)}-1\right]\right\}\,, \tag{38}$$

$$v^{(P)} := \overline{\langle p_{\text{F}}^{(P)}[v_m(t)]\rangle}$$

and

$$\langle S_m(t)S_n(t+r)\rangle = \langle p_{\text{F}}^{(P)}[v_m(t)]\rangle P\, p_n^{\text{in}}(t+r) \times \exp[\beta J_{mn}\epsilon(-r-\Delta_{mn})]\,. \tag{39}$$

We define the abbreviation $\lambda^{\text{struct}}(\mu) = \lambda(\mu) - \lambda^{\text{auto}} - \delta_{\mu 0}\lambda^{\text{post}}$ from (36) and find the following eigenvalues of the linearized dynamics with transmission probability P:

$$\lambda^{(P)}(\mu) = \frac{P\nu^{(P)}}{\nu^{\text{out}}}[P\lambda^{\text{struct}}(\mu) + \lambda^{\text{auto}} + \delta_{\mu 0}\lambda^{\text{post}}]\,.$$

The growth rate due to self-correlations λ^{auto} stems from the exponential function on the right-hand side of (39). The ratio $\lambda^{\text{auto}}/[P\lambda^{\text{struct}}(\mu)]$ is increased with increasingly unreliable synaptic transmission.

As a result, low transmission probabilities P reduce the driving force for the emergence of temporal structures, and therefore are disadvantageous from a point of view of optimizing temporal precision. They nevertheless can have a beneficial effect if one considers axonal and postsynaptic dendritic delays separately. Then, as shown by Senn et al. (2002), $P < 1$ can break up the degeneracy of eigenspaces, which is due to the fact that the learning rule is sensitive to time *differences* and, to a first-order approximation, cannot distinguish between synapses with equal difference between axonal and retrograde dendritic delays (cf. Senn 2002).

10 Conclusion

Mapping time by means of delay lines is restricted to temporal features occurring on a timescale of a few milliseconds and less. It can be guaranteed through AMSL. The relative strength of the axonal interaction can thereby be as small as the inverse of the number of interacting postsynaptic neurons. The result of delay selection on the level of afferent axons are waves of postsynaptic excitation. A neuronal anatomy providing several directions of afferent arborization thus yields interference patterns, whose maxima represent *time differences* between activation of the input populations. In the simplest case of two input populations arboring into opposite directions, this gives rise to a realization of the Jeffress model.

The latter is biologically implemented in the laminar nucleus of barn owls, a neuronal structure that is responsible for mapping interaural time differences on a timescale of 10μs. Our model is consistent with findings on maturation of the laminar nucleus in young owls.

We suggest that AMSL is a key mechanism for inducing map formation whenever time is involved. The simple reason behind this suggestion is that temporal correlations of input activity are best preserved in afferent axons.

Acknowledgements. The authors thank Richard Kempter and Hermann Wagner for a most enjoyable collaboration on understanding of how temporal maps can be realized through AMSL. C.L. is partially supported by the Deutsche Forschungsgemeinschaft, grant no. KL 608/10-3 and HE 3252/1-3 (FG Hörobjekte).

References

Ash RB (1972) Real analysis and probability. Academic, New York, Sect 5.5, Chap 6

Bi G-Q, Poo M-M (1998) Synaptic modifications in cultured hippocampal neurons: dependence on spike timing, synaptic strength, and postsynaptic cell type. J Neurosci 18: 10464–10472

Bonhoeffer T, Staiger V, Aertsen A (1989) Synaptic plasticity in rat hippocampal slice cultures: local 'Hebbian' conjunction of pre- and postsynaptic stimulation leads to distributed synaptic enhancement. Proc Natl Acad Sci USA 86: 8113–8117

Carr CE (1993) Processing of temporal information in the brain. Annu Rev Neurosci 16: 223–243

Carr CE, Konishi M (1990) A circuit for detection of interaural time differences in the brain stem of the barn owl. J Neurosci 10: 3227–3246

Cash S, Zucker RS, Poo M-M (1996) Spread of synaptic depression mediated by presynaptic cytoplasmic signaling. Science 272: 998–1001

Eurich CW, Pawelzik K, Ernst U, Cowan JD, Milton JG (1999) A Hebbian learning rule for delay adaption in neural networks. Phys Rev Lett 82: 1594–1597

Fitzsimonds RM, Poo M-M (1998) Retrograde signaling in the development and modification of synapses. Physiol Rev 78: 143–170

Fitzsimonds RM, Song H-J, Poo M-M (1997) Propagation of activity-dependent synaptic depression in simple neural nerworks. Nature 388: 439–448

Gerstner W, Kempter R, van Hemmen JL, Wagner H (1996) A neuronal learning rule for sub-millisecond temporal coding. Nature 383: 76–78

Goda Y, Stevens CF (1998) Readily releasable pool size changes associated with long term depression. Proc Natl Acad Sci USA 95: 1283–1288

Hale J, Koçak H (1991) Dynamics and bifurcations. Springer, Berlin Heidelberg New York, Chap 9

Hebb DO (1949) The organization of behavior. Wiley, New York

Hemmen JL van (2000) Theory of synaptic plasticity. In: Moss F, Gielen S (eds) Handbook of biophysics, vol 4. Elsevier, Amsterdam, pp 771–823

Jeffress LA (1948) A place theory of sound localization. J Comp Physiol Psychol 41: 35–39

Kempter R, Gerstner W, van Hemmen JL, Wagner H (1998) Extracting oscillations: neuronal coincidence detection with noisy periodic spike input. Neural Comput 10: 1987–2017

Kempter R, Gerstner W, van Hemmen JL (1999) Hebbian learning and spiking neurons. Phys Rev E 59: 4498–4514

Kempter R, Leibold C, Wagner H, van Hemmen JL (2001) Formation of temporal feature maps by axonal propagation of synaptic learning. Proc Natl Acad Sci USA 98: 4166–4171

Ledermann W (1944) Asymptotic formulae relating to the physical theory of cristals. Proc R Soc Lond A 182: 362–377

Leibold C, Kempter R, van Hemmen JL (2001) Temporal map formation in the barn owl's brain. Phys Rev Lett 87: 248101

Leibold C, Kempter R, van Hemmen JL (2002) How spiking neurons give rise to a temporal-feature map: from synaptic plasticity to axonal selection. Phys Rev E 65: 051915

Reyes AD, Rubel EW, Spain WJ (1996) In vitro analysis of optimal stimuli for phase-locking and time-delayed modulation of firing in avian nucleus laminaris neurons. J Neurosci 16: 993–1007

Sanders JA, Verhulst F (1985) Averaging methods in nonlinear dynamical systems. Springer, Berlin Heidelberg New York

Senn W (2002) Beyond spike timing: the role of nonlinear plasticity and unreliable synapses. Biol Cybern 87: 344–355

Senn W, Schneider M, Ruf B (2002) Activity-dependent development of axonal and dendritic delays, or, why synapses should be unreliable. Neural Comput 14: 583–619

Sullivan WE, Konishi M (1986) Neural map of interaural phase difference in the owl's brainstem. Proc Natl Acad Sci USA 83: 8400–8404

Tao H-ZW, Zhang LI, Bi G-Q, Poo M-M (2000) Selective presynaptic propagation of long-term potentiation in defined neural networks. J Neurosci 20: 3233–3243

Verhulst F (1996) Nonlinear differential equations and dynamical systems, 2nd edn. Springer, Berlin Heidelberg New York

Zhang LI, Tao HW, Holt CE, Harris WA, Poo M-M (1998) A critical window for cooperation and competition among developing retinotectal synapses. Nature 395: 37–44